Available online at www.sciencedirect.com

SciVerse ScienceDirect

journal homepage: www.elsevier.com/locate/ijrefrig

A 1D model to predict ejector performance at critical and sub-critical operational regimes

WeiXiong Chen [a,b], Ming Liu [a], DaoTong Chong [a,*], JunJie Yan [a], Adrienne Blair Little [c], Yann Bartosiewicz [b]

[a] State Key Laboratory of Multiphase Flow in Power Engineering, Xi'an Jiaotong University, Xi'an 710049, China
[b] Université catholique de Louvain (UCL), Institute of Mechanics, Materials and Civil Engineering (iMMC), Place du Levant 2, B-1348, Louvain-la-Neuve, Belgium
[c] George W. Woodruff School of Mechanical Engineering, Georgia Institute of Technology, Atlanta, GA 30332-0405, USA

ARTICLE INFO

Article history:
Received 26 September 2012
Received in revised form
11 March 2013
Accepted 13 April 2013
Available online 25 April 2013

Keywords:
Ejector
1D model
Performance
Entrainment ratio
Sub-critical operation

ABSTRACT

This paper proposes a new 1D model to predict ejector performance at critical and sub-critical operational modes, while most previous 1D models have only predicted ejector performance at critical mode operation. Constant pressure mixing is assumed to occur inside the constant area section of the ejector at critical and sub-critical mode operation, and the effectiveness of the model is verified against four sets of experimental data that include different working fluids and geometries. The results show that the proposed model accurately predicts ejector performance over all ranges of operation, and is a useful tool for predicting ejector performance within larger refrigeration cycle models.

Modèle unidimensionnel utilisé pour prévoir la performance d'un éjecteur sous des conditions de fonctionnement critiques et sous-critiques

Mots clés : éjecteur ; modèle undimensionnel ; performance ; ratio d'entraînement ratio ; sous-critique fonctionnement

1. Introduction

The recent global climate has made it highly desirable to develop and utilize new environment-friendly technologies. One such technology uses widely available low-grade thermal energy from sources such as industrial processes, solar collectors, and automobile exhaust. Supersonic ejectors, used to compress flows using only low-grade heat, are considered to be

* *Corresponding author*. Tel./fax: +86 29 82665741.
E-mail address: dtchong@mail.xjtu.edu.cn (DaoTong Chong).
0140-7007/$ – see front matter © 2013 Elsevier Ltd and IIR. All rights reserved.
http://dx.doi.org/10.1016/j.ijrefrig.2013.04.009

Nomenclature

A	area, m^2
a	sonic velocity, m s^{-1}
C_p	specific heat of gas at constant pressure, kJ kg^{-1} K^{-1}
d	diameter, m
E_R	error
M	Mach number
m	mass flow rate, kg s^{-1}
P	pressure, bar
R_g	gas constant, kJ kg^{-1} K^{-1}
T	temperature, °C
V	velocity, m s^{-1}

Greek symbols

γ	$=C_p/C_v$
η	isentropic coefficient
ν	specific volume, m^3 kg^{-1}
Ψ	frictional coefficient
ω	entrainment ratio

Superscripts

*	critical mode operation of ejector

Subscripts

c	back pressure
d	diffuser
m	mixed flow
p	primary flow
s	secondary flow
t	nozzle throat
y	location where two streams start to mix
1	nozzle exit
2	constant area section

one of the economically feasible and environmentally-friendly applications for harnessing low-grade thermal energy. Many theoretical and experimental studies have been carried out to obtain the performance of such ejectors in their respective applications (Sun and Eames, 1995, 1996; Aphornratana and Eames, 1997; Huang et al., 1998).

Depending on the position of the nozzle, there are two types of ejector designs (Sun and Emaes, 1996). When the nozzle exit is located within the constant area section of the ejector, and the mixing of primary and induced flows takes place in the constant area section, the ejector is known as "constant area mixing ejector." The other, known as "constant pressure mixing ejector," is when the nozzle exit is located before the mixing chamber, within a secondary convergent nozzle in front of the constant area section. The current work focuses on a constant-pressure mixing ejector because of its improved performance over a constant area mixing ejector.

Several mathematical models for ejectors have already been developed, usually based on 1D fluid dynamics theory and assuming that the radial velocities of both the primary and induced flows are uniformly distributed. To the authors' knowledge, the first such mathematical model was presented by Keenan and Neumann (1942). Their model was able to predict the performance of a constant area mixing ejector (without a diffuser), based on ideal gas dynamics and the principles of conservation of mass, momentum, and energy. Later, Keenan et al. (1950) introduced the concept of a constant pressure mixing ejector, and assumed that the pressures of the primary and induced flows are identical at the exit of the primary nozzle, and that the mixing of both streams starts at a uniform pressure up to the inlet of the constant area section without heat and friction losses. Munday and Bagster (1977) postulated a fictive throat or "effective area" located at a location inside the mixing chamber. They assumed that the primary flow fans out without mixing with the induced flow after discharging from the exit of nozzle such that the mixing process starts beyond the hypothetical throat with a uniform pressure. Based on their assumption, Huang et al. (1999) built a model on the assumption that constant pressure mixing occurs inside the constant area section of the ejector to predict performance during critical operation. More recently, the shock circle model proposed by Zhu et al. (2007) takes into account the nonuniformity of velocity by introducing a shock circle, however pressure was still assumed uniform in the radial direction. All of the above theoretical models were helpful in obtaining the ejector performance when the ejector was in critical operation, and the results agreed well with the experimental data. But predicting performance when the ejector is at sub-critical operation is also important for fields in industry, and the models mentioned above do not include such information.

More recent work has utilized CFD to study ejector performance (Hemidi et al., 2009; Bartosiewicz et al., 2005; Sriveerakul et al., 2007; Chen et al., 2011; Little et al., 2012). Most of the previous studies proved that CFD could accurately predict ejector performance at critical operation, but Sriveerakul et al. stated that CFD models failed to predict sub-critical operation since discrepancies of about 40–50% were reached. On the other hand, it should be noted that CFD methods are more complex and time consuming, requiring proper grid structuring and selection of a suitable turbulence model. On the contrary, a 1D model is computationally cheap and can rapidly obtain ejector performances over a large range of operation. Furthermore, 1D models are easily integrated into system models to predict overall operation of an ejector system.

To the authors' knowledge, previous theoretical studies usually focused on the prediction of the maximum entrainment ratio at critical mode operation, but ejector systems are not always operated at these conditions and require a model that can also predict performance at sub-critical conditions during transient or off-design conditions. The above 1D models are unable to predict such conditions, making it highly desirable to set up a model to predict ejector performance over all operational regimes. Ouzzane and Aidoun (2003) proposed a 1D model to obtain ejector performance at critical and sub-critical conditions based on a control volume method, but they

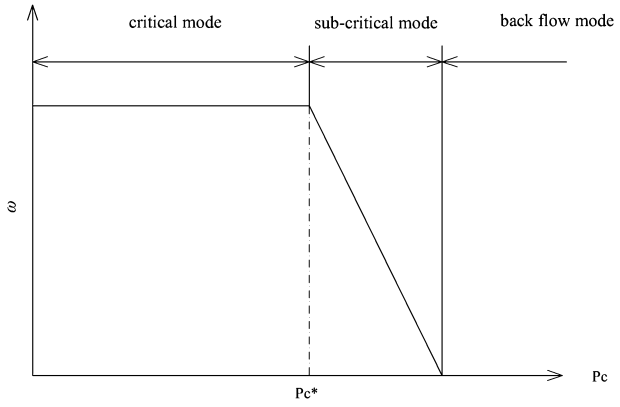

Fig. 1 – Ejector operational modes.

assumed a uniform pressure corresponding to the critical pressure of the secondary stream, and only validated their model for critical operation. However, when the ejector is at sub-critical operation, the uniform pressure is lower than the critical pressure. Boumaraf and Lallemand (2009) also proposed a 1D model to predict ejector performance at critical and sub-critical modes, but their model was based on constant area mixing theory, and the information about their assumptions on their sub-critical model is not clear. Chen et al. (2010) proposed a model to predict the entrainment ratio at sub-critical operation, but the information given on the model is not sufficient to evaluate its formulation or effectiveness.

The literature review above indicates that there are few studies dealing with the performance at sub-critical mode using theoretical analysis. In present study, a 1D model is proposed to predict the ejector performance not only at critical mode operation, but also at sub-critical mode operation. For validation purposes, the 1D model results are compared to existing experimental data from the literature not only for the critical mode and also for the sub-critical mode, as well as data collected by the authors from a large-scale ejector facility.

2. Theoretical analysis of ejector performance

In supersonic ejector applications, the most important indication of ejector performance is the entrainment ratio, defined as

$$\omega = \frac{m_s}{m_p}, \tag{1}$$

To evaluate performance in terms of entrainment ratio, ejector operation can be divided into three operational modes. Fig. 1 shows the variation in entrainment ratio with back pressure when the primary and induced pressures are fixed. During critical mode operation, the primary and induced flows are both choked, and the entrainment ratio reaches a maximum value that stays constant with lower values of back pressure. For sub-critical mode operation, only the primary flow is choked and the entrainment ratio changes with the back pressure. For the back flow mode, the induced flow is reversed and the entrainment ratio is less than zero.

Fig. 2 shows a schematic of a typical ejector. As the high-pressure stream, usually known as "primary flow," passes through the primary nozzle, it fans out at supersonic velocities at the exit of the primary nozzle (section 1-1). As a result of the low-pressure environment created by the supersonic primary flow and viscous entrainment effect, the induced flow is entrained into the mixing chamber. The primary flow expands and forms a converging duct for the induced flow before any mixing occurs with it, following the assumption used in Munday and Bagster (1977). As a result, the induced flow is accelerated to a sonic speed within the constant area section. After that, the mixing process begins when the induced flow chokes for critical mode operation, as proposed by Huang et al. (1999). In the present model, the hypothetical throat still occurs inside the constant-area section when the ejector is at critical mode operation. Furthermore, for the case of sub-critical mode operation, it is assumed that there also exists an effective area where the velocity of the induced flow is the highest (lower than the sonic speed), then the two streams mix at uniform pressure. It means that there always exits an effective area (section y–y) whether the ejector is at critical mode or not. The mixing process begins just after this section. The mixed fluid undergoes a normal shock at section N–N in the constant area section, which causes a major compression effect and a sudden drop in the flow speed. Finally, the mixture passes through the diffuser where the velocity is gradually reduced and pressure is recovered.

The following assumptions are made for the analysis:

1. The working fluid is an ideal gas with constant properties C_p and γ.
2. The flow inside the ejector is steady and one dimensional.

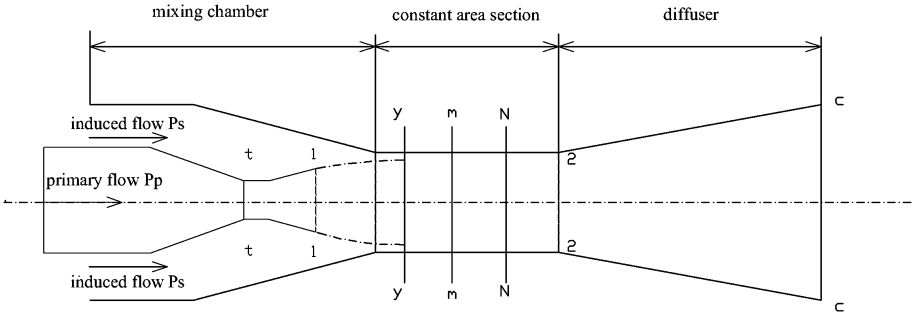

Fig. 2 – Schematic diagram of ejector performance.

3. The kinetic energy at the primary and induced flow inlets, as well as the exit of diffuser, are negligible.
4. For simplicity, when deriving the 1D model, isentropic relations are used as an approximation. But to account for non-ideal processes, the effects of frictional and mixing losses are accounted for with the use of isentropic efficiency coefficients.
5. After exiting the primary nozzle, the primary flow fans out without mixing with the induced flow up to at a certain cross section (y–y) inside the constant area section, irrespective of whether ejector is in the critical or sub-critical mode. Beyond this section, the two streams start to mix with a uniform pressure.
6. The inner wall of the ejector is adiabatic.

The above assumptions are almost similar with the other 1D models, with the exception of assumption (5).

2.1. Primary flow in the nozzle and suction chamber

For a given inlet total pressure, P_p, and temperature, T_p, the mass flow rate of primary flow through the nozzle, m_p, is obtain using the isentropic flow relation

$$m_p = \frac{P_p A_t}{\sqrt{T_p}} \times \sqrt{\frac{\gamma}{R}\left(\frac{2}{\gamma+1}\right)^{(\gamma+1)/(\gamma-1)}} \sqrt{\eta_p}, \tag{2}$$

where η_p is the isentropic efficiency coefficient for the nozzle. Applying conservation of mass and energy, the gas dynamic relations for isentropic flow relations between the Mach number at the exit of the nozzle, M_{p1}, the exit cross section area, A_{p1}, and the exit pressure, P_{p1}, are given by

$$\left(\frac{A_{p1}}{A_t}\right)^2 = \frac{1}{M_{p1}^2}\left[\frac{2}{\gamma+1}\left(1+\frac{\gamma-1}{2}M_{p1}^2\right)\right]^{(\gamma+1)/(\gamma-1)}, \tag{3}$$

$$\frac{P_p}{P_{p1}} = \left(1+\frac{\gamma-1}{2}M_{p1}^2\right)^{\gamma/(\gamma-1)}, \tag{4}$$

Since the primary flow fans out without mixing with the induced flow, the primary flow between sections 1-1 and y–y is approximated with isentropic relations, and the Mach number, M_{py}, of the primary flow at the y–y section is obtained with

$$\frac{P_{py}}{P_{p1}} = \frac{\left(1+((\gamma-1)/2)M_{p1}^2\right)^{\gamma/(\gamma-1)}}{\left(1+((\gamma-1)/2)M_{py}^2\right)^{\gamma/(\gamma-1)}}, \tag{5}$$

and the area of primary flow at y–y section, A_{py}, can be calculated using the following relation:

$$\frac{A_{py}}{A_{p1}} = \frac{\left(\eta_{py}/M_{py}\right)\left[(2/(\gamma+1))\left(1+((\gamma-1)/2)M_{py}^2\right)\right]^{(\gamma+1)/(2(\gamma-1))}}{(1/M_{p1})\left[(2/(\gamma+1))\left(1+((\gamma-1)/2)M_{p1}^2\right)\right]^{(\gamma+1)/(2(\gamma-1))}}. \tag{6}$$

The isentropic efficiency coefficient, η_{py}, is included to account for the losses of primary flow between sections 1-1 and y–y

$$\frac{T_p}{T_{py}} = 1+\frac{\gamma-1}{2}M_{py}^2. \tag{7}$$

2.2. Induced flow from inlet to section y–y

2.2.1. Critical mode

For critical mode operation, it is assumed that the induced flow chokes at section y–y. Under this condition, the following equations are valid:

$$M_{sy} = 1, \tag{8}$$

$$P_{sy} = P_{sy}^*, \tag{9}$$

and for a given total pressure P_s, P_{sy}^* is found from

$$P_{sy}^* = P_s\left(1+\frac{\gamma-1}{2}M_{sy}^2\right)^{-\gamma/(\gamma-1)} \tag{10}$$

For a given total pressure, P_s, and temperature, T_s, η_s is the isentropic efficiency coefficient for the induced flow, the mass flow rate of induced flow through the nozzle, m_s, is obtained at critical mode operation:

$$m_s = \frac{P_s A_{sy}}{\sqrt{T_s}} \times \sqrt{\frac{\gamma}{R}\left(\frac{2}{\gamma+1}\right)^{(\gamma+1)/(\gamma-1)}} \sqrt{\eta_s}. \tag{11}$$

2.2.2. Sub-critical mode

For sub-critical mode operation, it is assumed that there is an effective area where the velocity of the induced flow is the highest (but lower than the speed of sound in this case). As such, the following equations are valid:

$$M_{sy} < 1, \tag{12}$$

$$P_{sy} > P_{sy}^*, \tag{13}$$

Using conservation of mass and energy, as well as isentropic relations, the following equations are obtained:

$$\frac{T_{sy}}{T_s} = \left(\frac{P_{sy}}{P_s}\right)^{(\gamma-1)/\gamma}, \tag{14}$$

$$P_{sy}\nu_{sy} = RT_{sy}, \tag{15}$$

$$V_{sy} = \sqrt{2C_p(T_s - T_{sy})}, \tag{16}$$

$$m_s = \frac{V_{sy}A_{sy}}{\nu_{sy}}\sqrt{\eta_s}, \tag{17}$$

where η_s is the isentropic efficiency coefficient the secondary nozzle. The area of section y–y is A_2 where

$$A_{py} + A_{sy} = A_2. \tag{18}$$

A_{py} and A_{sy} are the areas for primary and induced flow, respectively.

2.3. Mixed flow at section m–m upstream of the shock

Both streams start to mix after section y–y. Applying a momentum and energy balance between sections y–y and m–m, the equations include

$$\psi_m(m_p V_{py} + m_s V_{sy}) = (m_p + m_s)V_m, \tag{19}$$

$$m_p\left(C_p T_{py} + \frac{V_{py}^2}{2}\right) + m_s\left(C_p T_{sy} + \frac{V_{sy}^2}{2}\right) = (m_p + m_s)\left(C_p T_m + \frac{V_m^2}{2}\right), \tag{20}$$

where V_m is the velocity of the mixed flow and ψ_m is the coefficient accounting for the frictional losses (Aphornratana and Eames, 1997;Huang et al., 1999). V_{py} and V_{sy} are the gas velocities of primary and induced flows at section y–y, and can be derived as

$$V_{py} = M_{py} a_{py}, \tag{21}$$

$$a_{py} = \sqrt{\gamma R T_{py}}. \tag{22}$$

The Mach number of the mixed flow can be evaluated using the following relations:

$$M_m = \frac{V_m}{a_m}, \tag{23}$$

$$a_m = \sqrt{\gamma R T_m}. \tag{24}$$

2.4. Mixed flow across the shock from section m–m to 2–2

A normal shock is set to exist at section N–N. Assuming that the mixed flow after the shock undergoes an isentropic process, the mixed flow between sections m–m and 2–2 inside the constant area section has a uniform pressure, P_2. Therefore, the gas dynamic relations are

$$\frac{P_2}{P_m} = 1 + \frac{2\gamma}{\gamma + 1}(M_m^2 - 1), \tag{25}$$

$$M_2^2 = \frac{1 + \frac{\gamma - 1}{2} M_m^2}{\gamma M_m^2 - \frac{\gamma - 1}{2}}. \tag{26}$$

2.5. Mixed flow through diffuser

Further pressure recovery of the mixed fluid is achieved as it passes through the subsonic diffuser, assuming isentropic process:

$$\frac{P_c}{P_2} = \left(1 + \frac{\gamma - 1}{2} M_2^2\right)^{\gamma/(\gamma-1)}. \tag{27}$$

2.6. Procedure

For a given nozzle throat diameter d_t (or area of nozzle throat A_t), nozzle exit diameter d_1 (or area of nozzle exit A_1), and constant area section diameter d_2 (or area of constant area section A_2), the performance of an ejector is characterized by the total pressure and temperature at the primary nozzle inlet (P_p, T_p), and the total pressure and temperature (P_s, T_s) at the suction chamber inlet. The numerical procedure follows the flowchart shown in Fig. 3. A critical step is to calculate the value of P_c^*, then gives a back pressure value P_c. If P_c is lower than P_c^*, the ejector is at critical operation. Otherwise, the ejector is at sub-critical operation. The output of the analysis includes the primary mass flow rate m_p, the secondary mass flow rate m_s, and the entrainment ratio ω. In the present model, all the default coefficients are taken from Huang et al. (1999). The coefficients accounting for the losses in the primary flow nozzle and from the exit of the nozzle to the section y–y are taken as $\eta_p = 0.95$ and $\eta_{py} = 0.88$, respectively. The coefficient accounting for the loss in the induced flow is taken as $\eta_s = 0.85$. The coefficient accounting for the frictional loss in

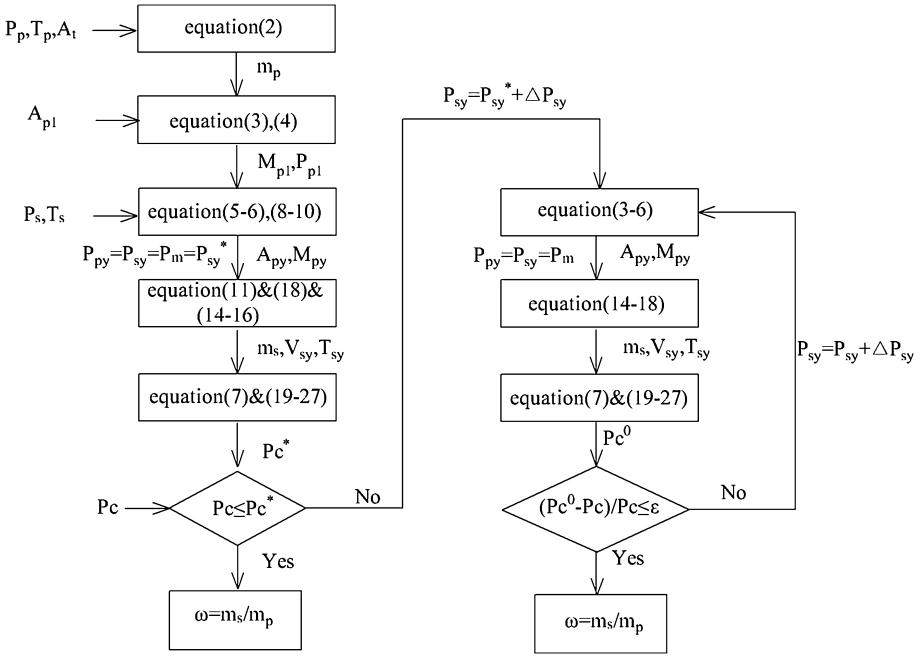

Fig. 3 – Calculation flowchart for current 1D model.

Table 1 – Comparison of performance between present model and experimental data of Huang et al. (1999). E_R = (theory-experiment)/experiment.

P_p (bar); T_p (°C)	P_s (bar); T_s (°C)	P_c (bar); T_c (°C)	Huang et al. 1D model ω	Experimental ω	Present model ω	1D E_R (%)	Present E_R (%)
A–A ejector							
6.04; 95	0.4; 8	1.42; 42.1	0.1554	0.1859	0.1595	−16.43	−14.20
5.38; 90	0.4; 8	1.28; 38.9	0.2156	0.2246	0.2050	−3.99	−8.73
4.65; 84	0.4; 8	1.14; 35.5	0.2880	0.2880	0.2705	0.23	−6.08
4; 78	0.4; 8	1.03; 32.5	0.3525	0.3257	0.3491	8.24	7.18
6.04; 95	0.473; 12	1.44; 42.5	0.2573	0.2350	0.2250	9.49	−4.26
5.38; 90	0.473; 12	1.31; 39.5	0.3257	0.2946	0.2787	10.54	−5.40
4.65; 84	0.473; 12	1.16; 36.0	0.4147	0.3398	0.3559	22.04	4.74
A–B ejector							
5.38; 90	0.4; 8	1.22; 37.5	0.2093	0.2718	0.2483	−22.99	−8.65
4.65; 84	0.4; 8	1.07; 33.6	0.3042	0.3117	0.3202	−2.39	2.73
4; 78	0.4; 8	0.93; 29.5	0.4422	0.3922	0.4063	12.74	3.60
A–G ejector							
6.04; 95	0.4; 8	1.27; 38.6	0.2144	0.2552	0.2505	−15.98	−1.84
5.38; 90	0.4; 8	1.19; 36.7	0.2395	0.3040	0.3065	−21.22	0.82
4.65; 84	0.4; 8	1.02; 32.3	0.3704	0.3883	0.3870	−4.61	−0.33
4; 78	0.4; 8	0.91; 29.1	0.4609	0.4393	0.4833	4.93	10.02
6.04; 95	0.473; 12	1.27; 38.7	0.3434	0.3503	0.3311	−1.97	−5.48
5.38; 90	0.473; 12	1.16; 36.0	0.4142	0.4034	0.3970	2.67	−1.59
4.65; 84	0.473; 12	1.03; 32.4	0.4769	0.4790	0.4917	12.09	2.65
4; 78	0.473; 12	0.92; 29.2	0.6659	0.6132	0.6050	8.60	−1.34
A-C ejector							
6.04; 95	0.4; 8	1.17; 36.3	0.2983	0.2814	0.2898	6.01	2.99
5.38; 90	0.4; 8	1.08; 33.8	0.3552	0.3488	0.3503	1.84	0.43
4.65; 84	0.4; 8	0.96; 30.5	0.4605	0.4241	0.4373	8.58	3.11
4; 78	0.4; 8	0.84; 26.9	0.5966	0.4889	0.5413	22.03	10.72
A–D ejector							
6.04; 95	0.4; 8	1.07; 33.6	0.3476	0.3457	0.3693	0.56	6.83
5.38; 90	0.4; 8	0.99; 31.5	0.4178	0.4446	0.4390	−6.02	−1.26
4.65; 84	0.4; 8	0.88; 28.0	0.5215	0.5387	0.5390	−3.19	0.06
4; 78	0.4; 8	0.77; 24.4	0.6944	0.6227	0.6586	11.51	5.77
6.04; 95	0.473; 12	1.10; 34.5	0.4708	0.4541	0.4698	3.67	3.46
5.38; 90	0.473; 12	1.01; 32.0	0.5573	0.5422	0.5516	2.78	1.73
4.65; 84	0.473; 12	0.91; 28.9	0.6906	0.6350	0.6691	8.75	5.37
4; 78	0.473; 12	0.81; 25.7	0.8626	0.7412	0.8095	16.37	9.21
E-G ejector							
6.04; 95	0.4; 8	1.37; 41.0	0.1919	0.2043	0.1831	−6.06	−10.38
E–C ejector							
6.04; 95	0.4; 8	1.28; 38.8	0.2078	0.2273	0.2176	−8.57	−4.27
6.04; 95	0.473; 12	1.30; 39.3	0.3235	0.3040	0.2927	6.41	−3.72
E–D ejector							
6.04; 95	0.4; 8	1.21; 37.1	0.2658	0.2902	0.2872	−8.39	−1.03
E–E ejector							
6.04; 95	0.4; 8	1.09; 34.2	0.3253	0.3505	0.3522	−7.20	0.49
6.04; 95	0.473; 12	1.09; 34.2	0.4894	0.4048	0.4498	10.55	11.12
E–F ejector							
6.04; 95	0.4; 8	1.05; 33.0	0.3774	0.3937	0.3985	−4.13	1.22
6.04; 95	0.473; 12	1.05; 33.1	0.5482	0.4989	0.5038	9.89	0.98
E–H ejector							
6.04; 95	0.4; 8	0.99; 31.3	0.4627	0.4377	0.4561	5.70	4.20

the mixing section, ψ_m, is sensitive to the area ratio, A_2/A_t, such that the empirical relation presented is used:

$$\psi_m = \begin{cases} 0.80, & \text{for } A_2/A_t > 8.3, \\ 0.82, & \text{for } 6.9 \le A_2/A_t \le 8.3, \\ 0.84, & \text{for } A_2/A_t < 6.9, \end{cases} \quad (28)$$

As mentioned above, all of the equations are similar with the model proposed by Huang et al. (1999) because of the same classic 1D theory based on the mass, momentum and energy conservation equations. But the detailed procedure flowchart at critical mode is different. In Huang's model, the critical back pressure P_c^* is an independent parameter (obtained from experimental data), and then the solution procedure is iterated until the theoretical critical back pressure equals to the experimental P_c^* by changing A_2 (the area of constant area section). Therefore, the entrainment

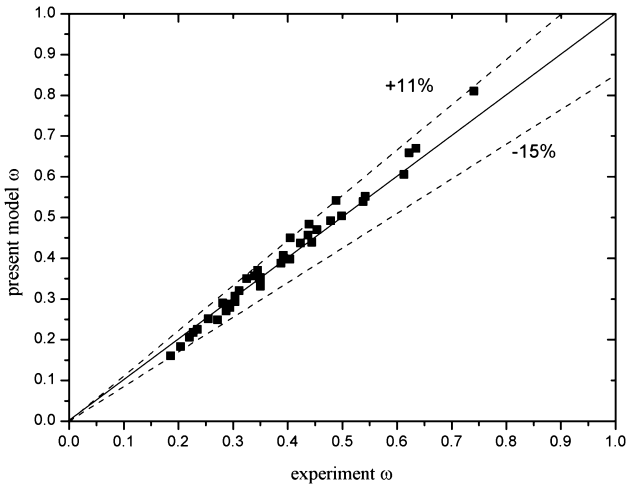

Fig. 4 – Entrainment ratio comparison of present model with experimental data from Huang et al. (1999).

ratio is calculated using the theoretical A_2 or required A_2 (not the experimental result A_2). Their purpose was to obtain the relation between the required A_2 and primary pressure and critical back pressure. In the present model, the critical back pressure P_c^* is not set as independent parameter, the entrainment ratio is calculated using the experimental A_2 value, and P_c^* is an output variable. The main purpose of the present paper is to predict the ejector performance over the entire range of operations for fixed ejector geometry.

3. Model validation

To validate the ability of the present model to predict entrainment ratio at critical mode operation, the experimental data of Huang et al. (1999) is used for comparison. The present model is then compared to data at critical and sub-critical mode operation from Hemidi et al. (2009) for an air ejector with a circular cross-section, as well as new experiments on a large-scale air ejector with a rectangular cross-section. Finally, the experimental data of a propane ejector embedded in an air-conditioning cycle are also used to verify the current model.

3.1. Comparison to Huang et al. (1999)

The experimental data collected by Huang et al. (1999) includes critical mode operation data points for a wide range of geometries with circular cross-sections, including two different primary nozzles with different throat (2.64 and 2.82 mm) and exit diameters (4.5 mm, 5.1 mm), and eight mixing tubes with different diameters (6.70–9.20 mm). Operating conditions include saturated generator vapor temperatures from 78 to 95 °C, and evaporator temperatures from 8 to 12 °C, and condenser temperatures from 24.4 to 42.5 °C. All of these temperatures represent the saturated vapor temperature of the corresponding pressures. The performances of the eleven different ejectors are obtained, all at critical mode operation.

The present model is set to have the same geometry and inlet/outlet conditions as the Huang et al. (1999) nozzles, and isentropic efficiency coefficients are taken to be the values indicated in Section 2.6. The properties of the working fluid R141b, such as C_p and γ, are computed by the NIST database (2005). Table 1 presents errors in entrainment ratio with respect to the experimental data, and shows that the results of the proposed model are also close to the experimental data. Compared to the experimental data, the largest error in the present model is less than 15% as shown Fig. 4. Therefore, the present model could accurately predict the ejector performances at critical mode, and has almost the same accuracy with the 1D model provided by Huang et al. (1999).

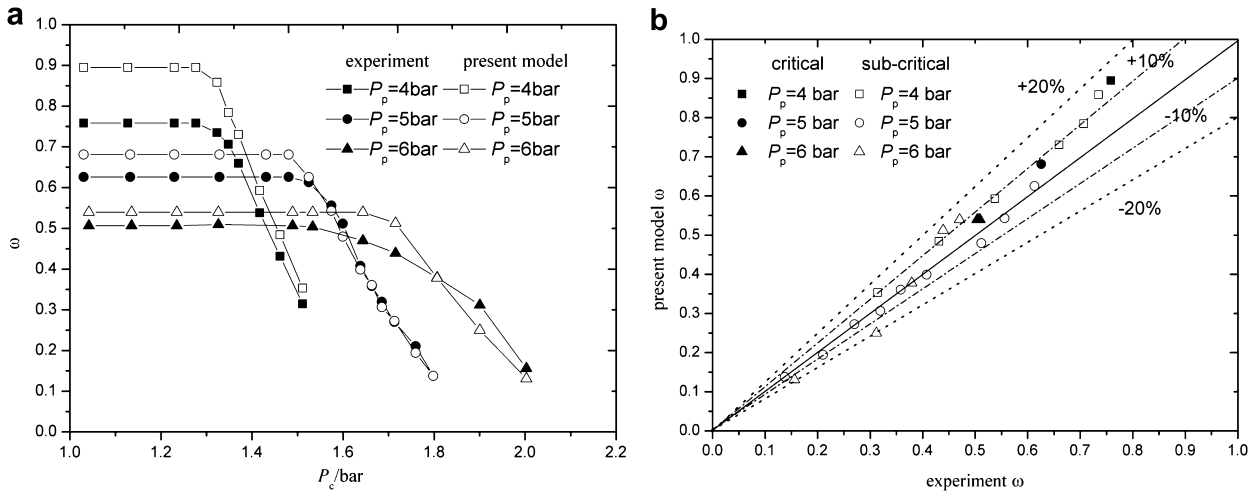

Fig. 5 – Entrainment ratio comparison of present model and experimental data from Hemidi et al. (2009): (a) comparison of characteristic curves, and (b) comparison of calculated errors.

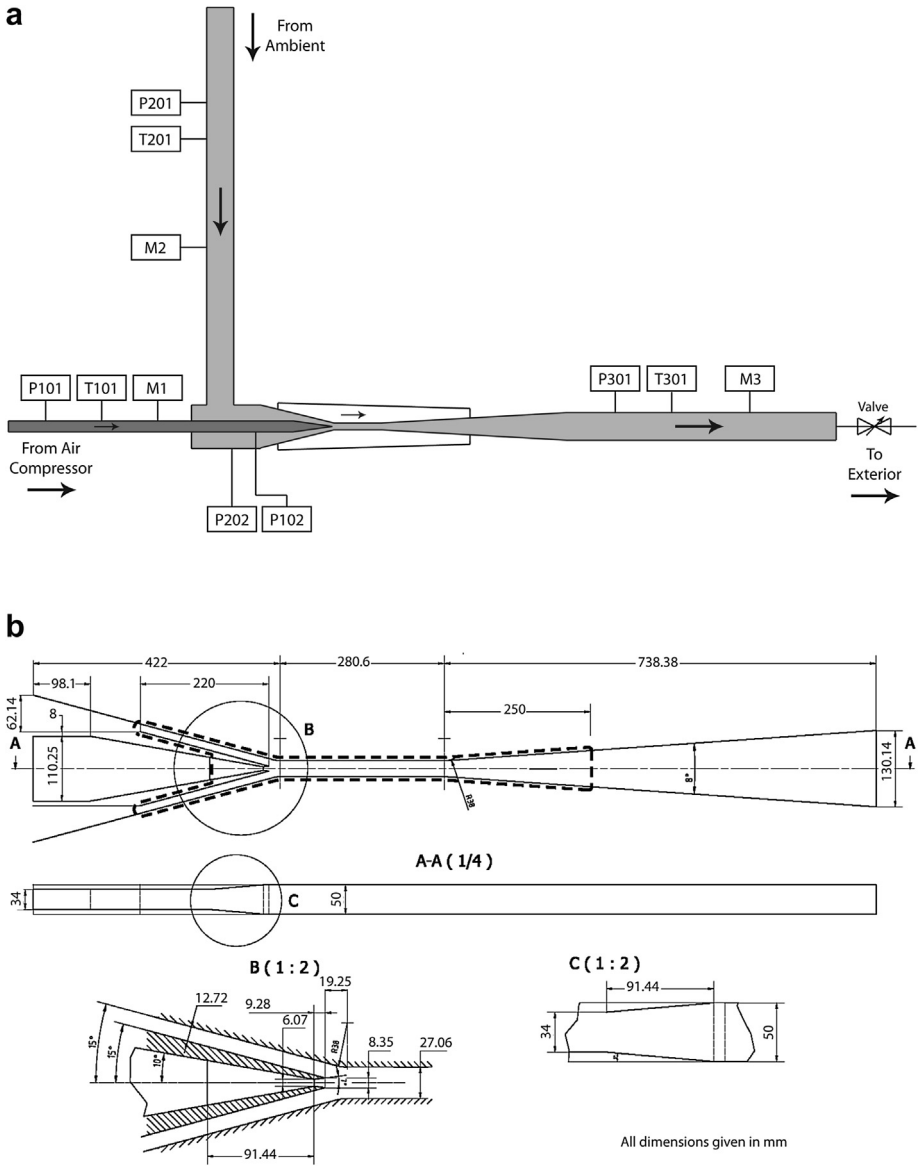

Fig. 6 – Schematic diagram of the ejector system (a) and experimental ejector (b).

3.2. *Comparison to Hemidi et al. (2009)*

In order to verify the proposed model at not just critical mode, but also sub-critical mode operation, experimental data from Hemidi et al. (2009) is used from an air ejector with a circular cross-section. The geometry characteristics of the air ejector are $d_t = 3.3$ mm, $d_1 = 4.5$ mm, $d_2 = 7.6$ mm. The primary pressure ranges from 4 to 6 bar, and the back pressure ranges from 1 to 2 bar. It is indicated that the induced pressure was roughly constant for all tests, and equal to the atmospheric pressure ($\approx$1 bar). Inlet and outlet temperatures for the ejector were not given, so the temperatures of the primary and induced flows are assumed to be 20 °C.

The present model is configured to have the same geometry and conditions as given in Hemidi et al. (2009), and the isentropic efficiency coefficients are set to be the values indicated in Section 2.6. The ejector is tested under three different motive pressures, and for each motive pressure, the performance is obtained with varying back pressure. The theoretical results provided by the present model coincide fairly well with the experimental data, with the largest error being less than 19.8%, and most data points lying within ±10% error, as shown in Fig. 5a and b.

3.3. *Comparison to large-scale rectangular cross-section air ejector*

New experiments on a large-scale rectangular cross-section air ejector are also used to verify the present model. The large-scale air ejector set up for visualization research. Fig. 6a provides a schematic of the ejector, and the important geometry parameters are given in Fig. 6b. The ejector has a

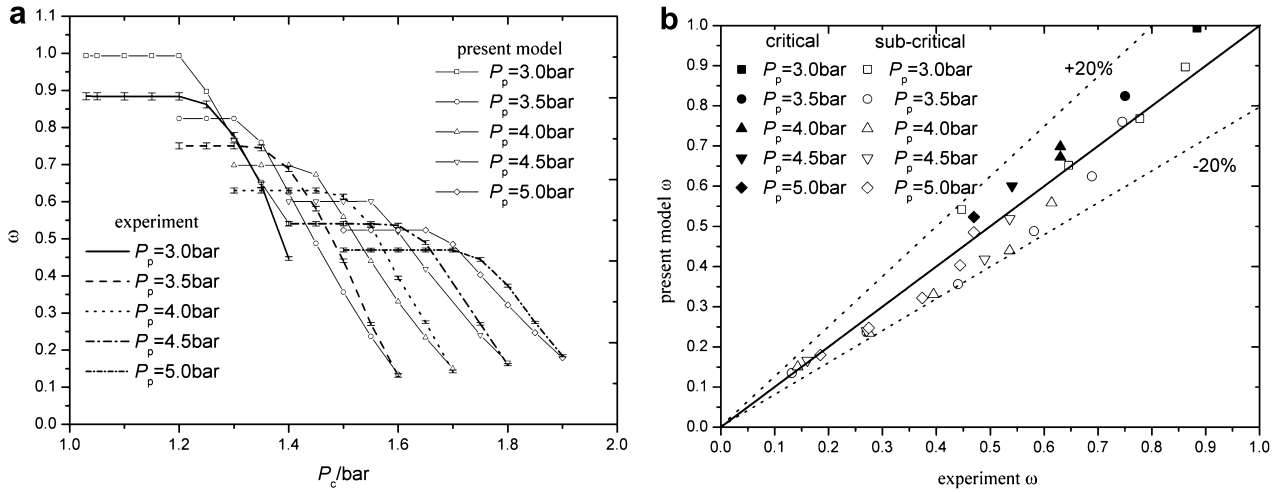

Fig. 7 – Entrainment ratio comparison of present model and experimental data from large-scale rectangular cross-section air ejector: (a) comparison of characteristic curves, and (b) comparison of calculated errors.

rectangular cross-section to avoid visual distortion effects, and the side walls are made of Plexiglas for optical access (for visualization experiments not related to this study). Air is supplied to the motive nozzle inlet by an industrial Ateliers François compressor (Model CE46B with a capacity of 1320 m^3 h FAD and power of 250 kW) and regulated by a Bellofram T-2000 pneumatic valve based on controller input. The maximum motive inlet pressure is limited to 6 bar, at which

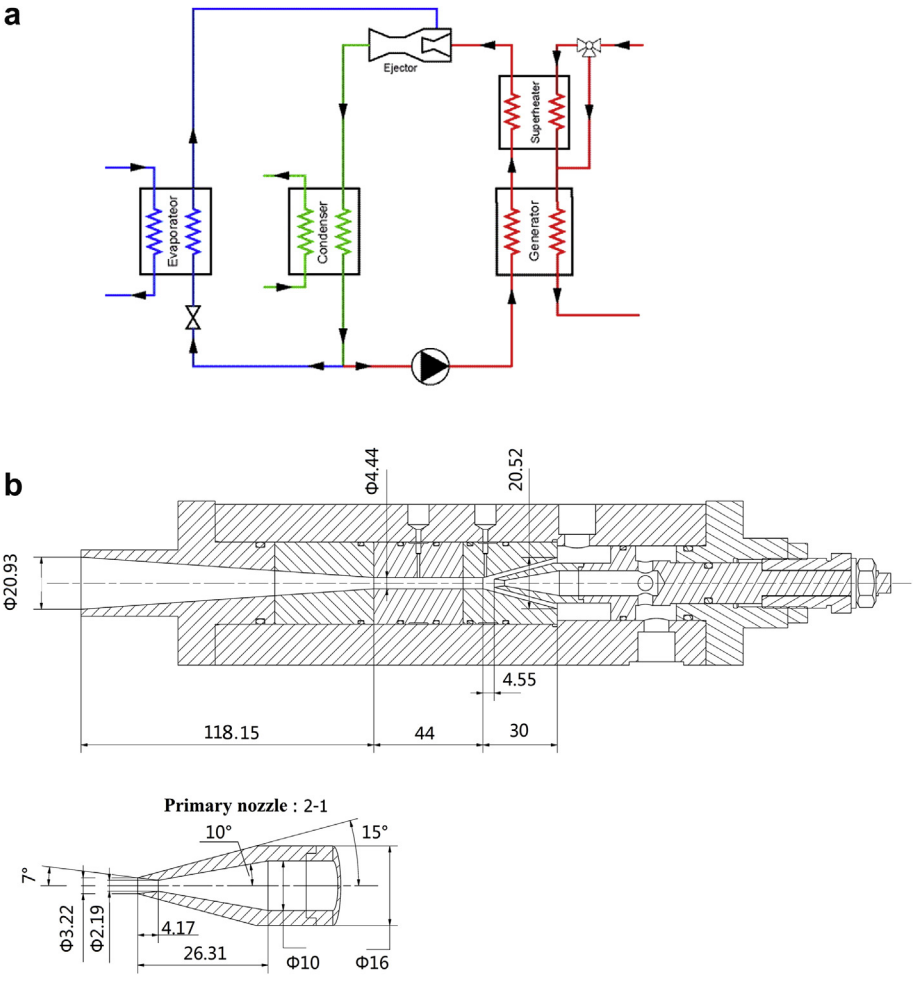

Fig. 8 – Schematic of (a) the propane ejector system and (b) experimental propane ejector component.

the maximum motive air mass flow rate is 0.35 kg s^{-1} while the primary pressure is from 3 to 5 bar. The induced flow is taken from the ambient for all test conditions, and based on the geometry of this specific ejector, the suction air mass flow rate can reach up to 0.18 kg s^{-1}. The outlet of the ejector also leads to the ambient, and a butterfly valve regulates the exit pressure of the visualization section between ambient pressure and the desired set point (1–2 bar). As shown in Fig. 6b, the height of the primary throat nozzle is 6.07 mm, the height of the primary nozzle exit is 8.35 mm, and the height of constant area section is 27.06 mm, while the width of the entire flow region is 50 mm.

Performance curves for the operation of this ejector are obtained by changing the back pressure at a constant primary and induced pressure. The pressures are measured with Endress Hauser and Kistler pressure transducers (uncertainty $< \pm 300$ Pa), and temperatures are measured with PT100 RTD temperature probes (uncertainty $< \pm 0.5$ °C). The mass flow rates are obtained using orifice plate device equipped with 1D and 1/2 D pressure taps according to the ISO 5167 standard, and the uncertainties for primary flow and induced flow were less than 0.79% and 3.47%, respectively.

The isentropic coefficients used in the present model are the default values in Section 2.6. As shown in Fig. 7a and b, the theoretical results of entrainment ratio are close to the experimental results under all primary pressures, with the largest error being less than 20%. These results indicate that the present model accurately predicts the performance of an air ejector with a rectangular cross-section over a range of operation.

3.4. *Comparison to ejector operating with propane*

As a last validation case, the present model is also used to predict the performance of an in-house test ejector embedded in a refrigeration cycle with propane as the working fluid. Fig. 8a shows a schematic diagram of the propane ejector and the system it is used in. The ejector refrigerator system consists of four main parts: generator, ejector, condenser, and evaporator. The generator produces saturated vapor by extracting heat from the boiler and delivers a power of 12 kW at temperatures between 60 and 95 °C. The primary flow is slightly superheated to avoid condensation inside the ejector, and then enters the ejector through a converging–diverging nozzle. The induced flow is entrained into the suction chamber from the evaporator, and the pressure of the evaporator can be changed based on the evaporation temperature between 10 and 15 °C. The primary flow and induced flow then mix in the ejector and finally discharge into the condenser, where the back pressure is then set by controlling the condenser temperature between 25 and 45 °C. The

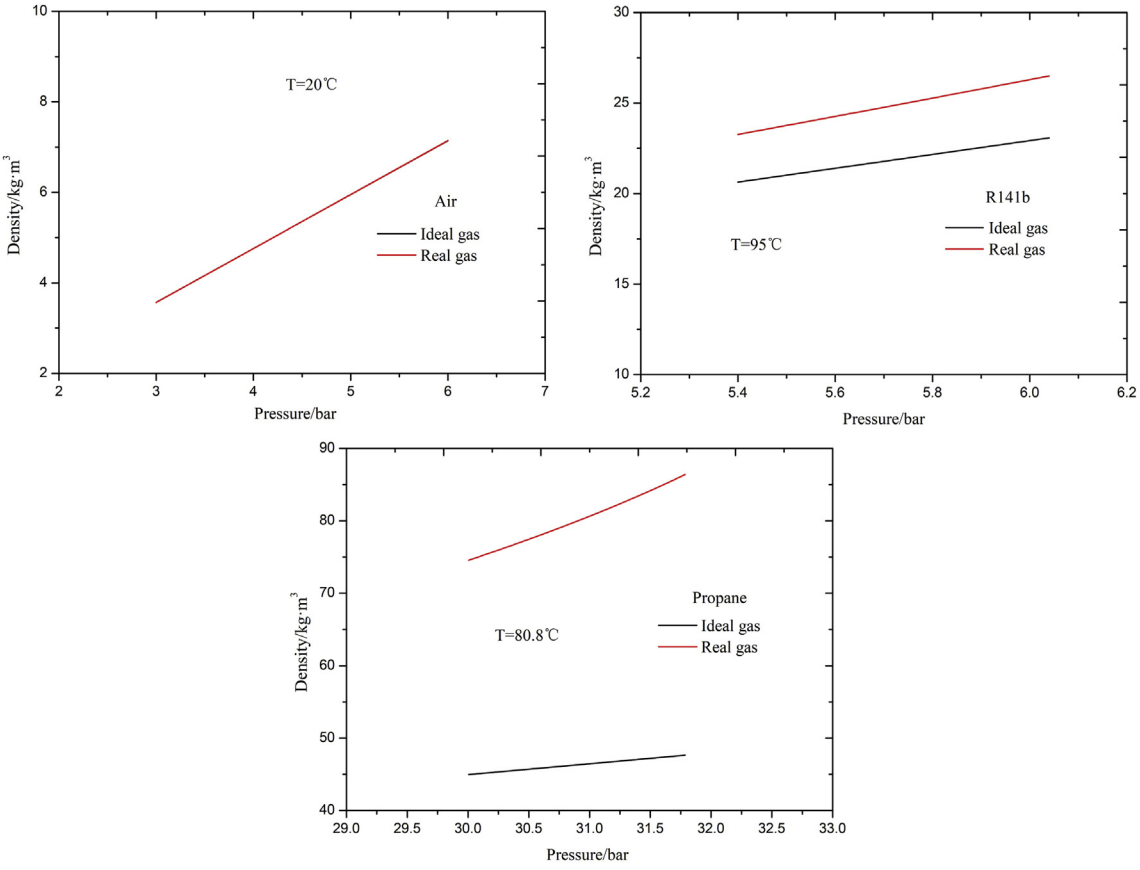

Fig. 9 – Comparison of ideal gas and real gas properties of three different working fluids.

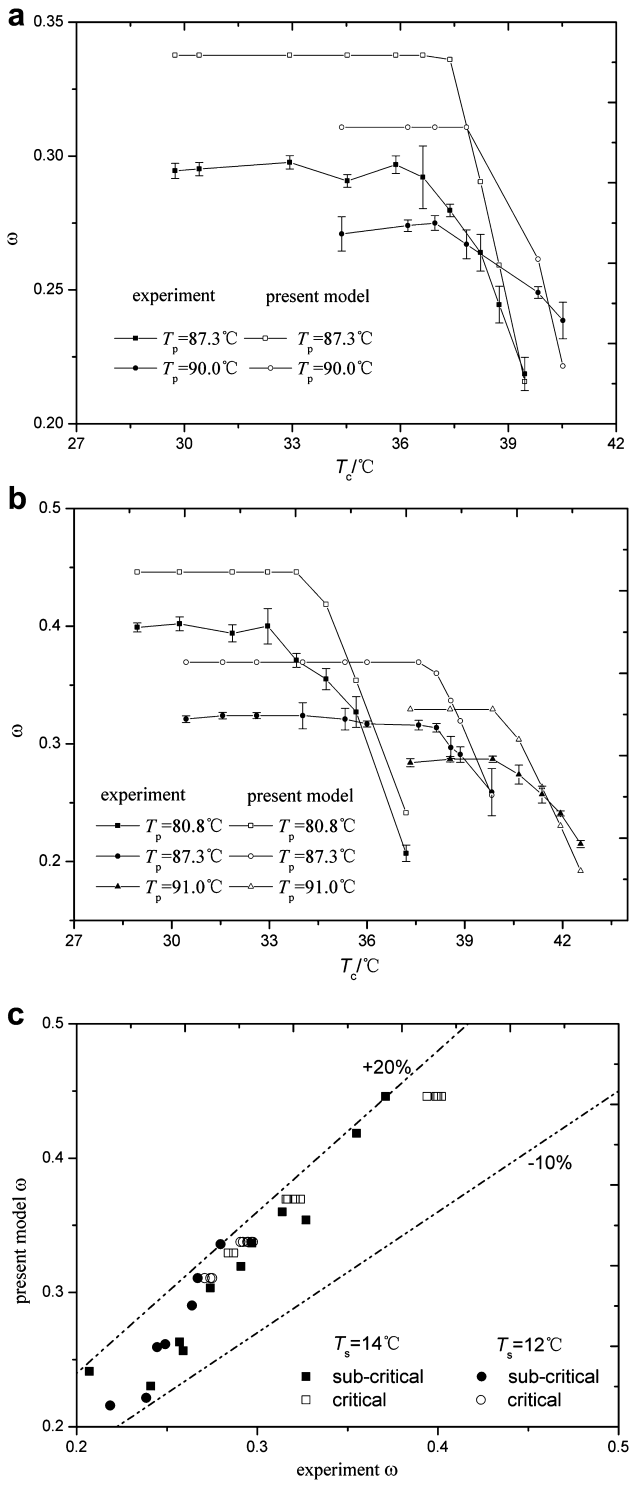

Fig. 10 – Entrainment ratio comparison of present model and experimental data for propane ejector: (a) comparison of characteristic curves for T_s = 12 °C, (b) comparison of characteristic curves for T_s = 14 °C, and (c) comparison of calculated error.

experimental ejector is a constant pressure mixing ejector, and the important geometry parameters are d_t = 2.19 mm, d_1 = 3.22 mm, d_2 = 4.44 mm.

Pressures are measured by pressure transducers with an uncertainty of <± 0.5% FS, and temperatures are measured with PT100 thermocouples with an uncertainty of <±0.1 °C. The mass flow rates are measured by Endress coriolis mass flowmeters, and the uncertainties for primary flow and induced flow were less than 3.82% and 7.24%, respectively.

The present model is applied for the same set of configurations, and the coefficients in the model are taken as η_p = 0.98, η_{py} = 0.95, η_s = 0.85, and ψ_m = 0.84. The coefficients differ from those for the previous comparisons because the properties of propane deviate more from the ideal gas law, especially at higher pressures. As shown in Fig.9, air and R141b could be treated as ideal gas, because the deviation between the ideal gas and real gas of these two fluids is not large. But for propane, properties deviate significantly from the ideal gas law at high pressure, justifying the change in coefficients used. The properties of propane, such as C_p and γ, are computed by the NIST database (2005). The ejector is tested for different primary, induced, and back pressures. In the figures, these conditions are indicated by the saturated temperature corresponding to the pressure. As shown in Fig. 10a and b, the present model predicts the entrainment ratios that agree very well with experimental results, not only for critical mode operation, but also for sub-critical mode operation such that the relative errors are all within ±20%, as shown in Fig. 10c. Moreover, all data from the present model are bigger than experimental results on critical operation, as shown in Figs. 5, 7a and 10a and b. The same phenomena also happen between the CFD results and experimental results from Hemidi et al. (2009). The way to reduce the errors is to adjust the isentropic efficiency.

4. Summary and conclusion

This study proposes a new model to predict ejector performance over all modes of operation, including both critical and sub-critical operation. Compared with the previous 1D models, the present model extends its capacity to predict the ejector performance at sub-critical mode, as well as the critical mode. Table 2 gives a summary of the ability of the present model to predict ejector performance. As shown in Table 2, the present model predicts the performance of ejectors with different geometries (different nozzle and mixing section diameters, circular and rectangular cross sections, large and small scale) and different working fluids (R141b, air, propane) via comparison with experimental data. It shows that the present model accurately predicts the ejector performance over the entire range of operation with errors <20% for all entrainment ratio comparisons performed. With such validation, the 1D model presented in this paper is ideal for integration into overall system models to accurately predict the critical and sub-critical performance of an ejector in refrigeration cycles,

Table 2 – Summary of the present model in predicting ejector performance.

Case	Working fluid	Cross-section type	d_t (A_t)	d_2 (A_2)	Maximum error	
					Critical mode	Sub-critical mode
1	R141b	Circular	2.64, 2.82 mm	6.20–9.20 mm	15%	/
2	Air	Circular	3.3 mm	7.6 mm	18%	20%
3	Air	Rectangular	303.5 mm^2	1353 mm^2	12%	20%
4	Propane	Circular	2.19 mm	4.44 mm	16%	20%

especially for sub-critical startup conditions that are inherent in transient ejector usage.

Acknowledgments

This work is supported by National Natural Science Foundation of China (No. 51006081 and No. 51125027), National Basic Research program of China (973 Program) (No. 2009CB219803).

REFERENCES

Aphornratana, S., Eames, I.W., 1997. A small capacity steam-ejector refrigerator: experimental investigation of a system using ejector with movable primary nozzle. Int. J. Refrigeration 20 (5), 352–358.

Bartosiewicz, Y., Aidoun, Z., Desevaux, P., Mercadier, Y., 2005. Numerical and experimental investigation on supersonic ejectors. Int. J. Heat Fluid Flow 26 (1), 56–70.

Boumaraf, L., Lallemand, A., 2009. Modeling of an ejector refrigerating system operating in dimensioning and off-dimensioning conditions with the working fluids R142b and R600a. App. Therm. Eng. 29 (2–3), 265–274.

Chen, G., Xu, X., Liu, S., Liang, L., Tang, L., 2010. An experimental and theoretical study of a CO_2 ejector. Int. J. Refrigeration 33 (5), 915–921.

Chen, W.X., Chong, D.T., Yan, J.J., Liu, J.P., 2011. Numerical optimization on the geometrical factors of natural gas ejectors. Int. J. Therm. Sci. 50 (8), 1554–1561.

Hemidi, A., Henry, F., Leclaire, S., Seynhaeve, J.M., Bartosiewicz, Y., 2009. CFD analysis of a supersonic air ejector. Part I: experimental validation of single-phase and two-phase operation. Appl. Therm. Eng. 29 (14–15), 2990–2998.

Huang, B.J., Chang, J.M., Petrenko, V.A., Zhuk, K.B., 1998. A solar ejector cooling system using refrigeration R141b. Sol. Energy 64 (4–6), 223–226.

Huang, B.J., Chang, J.M., Wang, C.P., Petrenko, V.A., 1999. A 1-D analysis of ejector performance. Int. J. Refrigeration 22 (5), 354–364.

Keenan, J.H., Neumann, E.P., 1942. A simple air ejector. J. Appl. Mech. Trans. ASME 64, A75–A81.

Keenan, J.H., Neumann, E.P., Lustwerk, F., 1950. An investigation of ejector design by analysis and experiment. J. Appl. Mech. Trans. ASME 17, 299–309.

Little, A.B., Bartosiewicz, Y., Garimella, S., 2012. Optical validation of ejector flow characteristics predicted by computational analysis. In: Proceedings of the IMECE 2012: ASME International Mechanical Engineering Congress & Exposition, Houston, Texas, USA.

Munday, J.T., Bagster, D.F., 1977. A new ejector theory applied to steam jet refrigeration. Ind. Eng. Chem. Process. Des. Dev. 16 (4), 442–449.

NIST Chemistry WebBook, 2005. release. NIST standard reference database number 69. http://webbook.nist.gov/chemistry.

Ouzzane, M., Aidoun, Z., 2003. Model development and numerical procedure for detailed ejector analysis and design. App. Therm. Eng. 23 (18), 2337–2351.

Sriveerakul, T., Aphornratana, S., Chunnanond, K., 2007. Performance prediction of steam ejector using computational fluid dynamics: part 1. Validation of the CFD results. Int. J. Therm. Sci. 46 (8), 812–822.

Sun, D.W., Eames, I.W., 1995. Recent developments in the design theories and applications of ejectors—a review. J. Inst. Energy 68, 65–79.

Sun, D.W., Emaes, I.W., 1996. Performance characteristics of HCFC-123 ejector refrigeration cycles. Int. J. Energy Res. 20 (10), 871–885.

Zhu, Y., Cai, W., Wen, C., Li, Y., 2007. Shock circle model for ejector performance evaluation. Energ. Convers. Manage 48 (9), 2533–2541.